Biomass waste fern leaves as a material for a sustainable method of activated carbon production for CO2 capture

Biomass and Bioenergy 175 (2023) 106880

Contents lists available at ScienceDirect

Biomass and Bioenergy

journal homepage: www.elsevier.com/locate/biombioe

Biomass waste fern leaves as a material for a sustainable method of activated carbon production for CO_2 capture

Jarosław Serafin [a,*], Bartosz Dziejarski [b,c], Xavier Vendrell [a], Karolina Kiełbasa [d], Beata Michalkiewicz [d]

[a] Department of Inorganic and Organic Chemistry, University of Barcelona, Martí i Franquès, 1-11, 08028, Barcelona, Spain
[b] Faculty of Environmental Engineering, Wroclaw University of Science and Technology, 50-370, Wroclaw, Poland
[c] Department of Space, Earth and Environment, Division of Energy Technology, Chalmers University of Technology, SE-412 96, Gothenburg, Sweden
[d] West Pomeranian University of Technology in Szczecin, Faculty of Chemical Technology and Engineering, Department of Catalytic and Sorbent Materials Engineering, Piastów Ave. 42, 71-065, Szczecin, Poland

ARTICLE INFO

Keywords:
Biomass recycling
Chemical and physical activation
Post-combustion CO_2 capture
Gas selectivity

ABSTRACT

In this work, we report the use of activated carbon synthesized from a sustainable material - fern leaves - as a sorbent for carbon dioxide capture applications. The resource-friendly technology for activated carbon production was applied and described. The activated carbons were prepared by chemical and physical activation and carbonization at the same time at the temperature range of 500–900 °C. This method reduces energy consumption and resources. KOH and CO_2 were used as activating agents. The evaluation of the CO_2 adsorption ability of the activated carbon was supported by different methods including: elemental analysis using X-ray fluorescence spectroscopy, ash content, surface area and porosity measurements, Raman spectroscopy, X-ray spectroscopy and scanning electron microscopy. Results indicated that the optimum temperature of the synthesis was 700 °C. The highest achieved adsorption of CO_2 was equal to 6.77 mmol/g and 3.58 mmol/g at 0 °C and 25 °C, respectively. The activated carbons synthesized from fern leaves showed high CO_2 adsorption and selectivity. Moreover, the abundance and low cost of fern leaves make them very promising carbon sources for CO_2 sorbents production.

1. Introduction

Biomass provides around 14% of the world's energy consumption, however a great amount of biomass has no application [1]. The biomass used for activated carbons synthesis with tailored physicochemical properties is a key idea for sustainable development. The great interest in the use of biomass as a carbon source is due to its abundance, low price, and renewability [2]. A large quantity of activated carbons produced from biomass has been applied as CO_2 sorbents [3,4].

Carbon dioxide is seen as one of the major anthropogenic factors related to greenhouse gas emissions. It is believed that the primary greenhouse gas is carbon dioxide (CO_2), which come from the energy industry, which relies on the burning of fossil fuels [5]. The increase in the concentration of CO_2 in the atmosphere will bring about visible climate changes. Despite the efforts and still developing science to find alternative methods of generating energy, fossil fuels remain the leading energy source. The need to capture and convert greenhouse gases, including mainly carbon dioxide, requires intensified research into the preparation of cheap, porous adsorbents and catalysts [6]. Among the various technologies proposed to reduce the amount of CO_2, the adsorption of this gas is very promising [7,8]. The efficiency of this process largely depends on the type of adsorbent used and the degree of development of its porous structure, including in particular, the degree of development of microporosity. Various porous materials were used for CO_2 adsorption, such as zeolites [9], organometallic compounds [10], modified mesoporous materials [11], MOFs [12], mesoporous silica-carbon composites [13] and, above all, activated carbons [14,15]. The latter is particularly important because they have a large specific surface area, a well-developed microporous structure, often defined pore morphology, and good chemical and thermal resistance.

The fern leaves are one of the ubiquitous biomass in a natural environment that can be applied as a carbon source for activated carbon production. Furthermore, the leaves of ferns may be regarded as superfluous matter, as they tend to accumulate as organic detritus when

* Corresponding author.
E-mail address: jaroslaw.serafin@qi.ub.es (J. Serafin).

https://doi.org/10.1016/j.biombioe.2023.106880
Received 2 November 2022; Received in revised form 15 June 2023; Accepted 18 June 2023
Available online 24 June 2023

they are shed or pruned from fern plants. Especially in gardening, landscaping, or agricultural practises, fern leaves that are pruned or removed as part of maintenance activities might be considered waste [16]. Regarding the potential for valorization, fern leaves can be reused and converted into valuable products such as activated carbon. This methodology has the potential to directly optimize the exploitation of biomass materials. However, certain factors and prospective issues require attention when establishing the worth of fern leaves for the purpose of producing activated carbon. Initially, it is imperative to address the existence of impurities in the fern leaves to avert the discharge of harmful substances during the treatment procedure. Comprehensive sourcing and pre-treatment protocols are imperative to guarantee the integrity of the raw materials. Secondly, the optimization of both yield and quality of activated carbon requires the consideration of various factors, including but not limited to the species of fern,the timing of harvesting, the process of carbonization, and the conditions of activation. Each parameter must be carefully controlled to achieve desired properties and maximize adsorption capacity. Overall, the successful valorization of fern leaves into activated carbon relies on thorough consideration of these factors, ensuring both effectiveness and sustainability.

Consequently, in the present work, fern leaves, a sustainable material, have been selected for activated carbon production and their role in post-combustion CO_2 adsorption. The sustainable technology of activated carbon production was widely examined by the authors. A novel one-step method was applied, namely, combined carbonization and chemical and physical activation (CChPA). Since both chemical and physical activation, as well as carbonization, take place simultaneously in the oven, the technique under consideration is environmentally friendly. This is an efficient approach in terms of its use of energy and resources. To our knowledge, this method has not been widely described until now in the literature, and there have been only a few studies on this subject. It's worth to underline that very high CO_2 adsorption was achieved: 6.77 mmol/g and 3.58 mmol/g at 0 °C and 25 °C, respectively.

2. Materials and methods

2.1. Preparation method

The activated carbons were prepared from fern biomass by CChPA method. KOH and CO_2 were used as chemical and physical activating agents respectively. The impregnation process consisted of mixing a saturated solution of potassium hydroxide with biomass for 1 h. Thus, the mass ratio of dry biomass: KOH was equal to 1:1. Afterwards, the mixture was dried in a quartz boat at 200 °C for 19 h. The CChPA was performed in a horizontal pipe furnace made of stainless steel from Czylok Company, Poland (PRW S 115/110) with 7.5 $dm^3\ h^{-1}$ carbon dioxide flow, with the rate of heating of 10 deg min^{-1} from ambient temperature to 500–900 °C and maintained at that temperature for 1 h. The samples were finally washed with deionized water, with 1 M HCl, and with deionized water again to eliminate chloride ions. After washing, activated carbons were dried at a temperature of 200 °C for 12 h. Finally, the material was grounded into a powder.

2.2. Characterization of carbon materials

The textural properties of activated carbons were determined by nitrogen adsorption/desorption at −196 °C. This characterization was carried out using automated volumetric apparatus Quadrasorb Evo™ Gas Sorption analyser (Quantachrome Instruments). All samples were outgassed at 250 °C during 16 h before the measurements. The specific surface areas (S_{BET}) were calculated using the Brunauer–Emmett–Teller (BET) equation based on of measurements at a relative pressure of 0.05–0.35. The total pore volume (V_{tot}) was calculated from the nitrogen amount adsorbed at a relative pressure, $p/p_0 = 0.99$. The micropore volume (V_{micN2}) for pores >1.4 nm received from N_2 adsorption at −196 °C and small micropore volume (V_{micCO2}) with diameters 0.3–1.4 nm received from CO_2 adsorption at 0 °C were determined using the DFT method.

The X-ray diffraction (XRD) patterns of the samples were recorded with an X-ray diffractometer (X'Pert–PRO, Panalytical) using Cu Kα lamp as the radiation source. The measurements were performed in the 2θ range 10–80° with a step size of 0.026.

The mean crystallite thickness (Lc) and the mean diameter of the graphene sheet (La) were approximately calculated using the empirical expression proposed by Scherrer (1) [17]:

$$L = \frac{K\lambda_{XRD}}{\beta\ cos(\theta_{hkl})} \tag{1}$$

where:

L – crystallite size along a line normal to the reflecting plane [nm],
λ_{XDR} - X-ray wavelength (0.154 nm for Cu),
K - constant depending on the reflection plane,
β - width at half the height of the peaks (100/101) or (002) after deduction of the apparatus correction [rad],
θ_{hkl} - reflection angle [rad].

The instrumental correction β_{inst} was subtracted from the measured peak width at half height β_{meas} using the Warren method, assuming that the peaks were Gaussian [15]:

$$\beta = \sqrt{\beta_{meas}^2 - \beta_{inst}^2} \tag{2}$$

To determine the size of the crystallites perpendicular to the graphene layers (Lc), the signal (002) was used, and the value of K was assumed to be 0.89. The size parallel to the graphene layers (La) was determined based on (100/101), assuming the value of K 1.84 [18].

Average graphite layer spacing was calculated using Bragg's law (3):

$$d_{002} = \frac{n\lambda_{XRD}}{2\ sin(\theta_{002})} \tag{3}$$

where:

n - the deflection order is usually taken to be equal to 1.

The number of graphite layers (N) was estimated by equation (4):

$$N = \frac{L_c}{d_{002}} \tag{4}$$

Raman spectroscopy was used to determine the structure of the carbon skeleton of the prepared carbon materials. Raman analysis was recorded on a InVia Raman Microscope (Renishaw PLC), with a laser wavelength of 785 nm. The spectrum obtained in the Raman shift range from 800 cm^{-1} to 2000 cm^{-1} was analysed. The Raman spectra were normalizing with respect to the G band. The values of G intensities were equal to the ratio of the intensity of the G peak to intensity of the D peak:

$$R = \frac{I_D}{I_G} \tag{5}$$

where:

I_D – is the intensity of the D peak;
I_G – is the intensity of the G peak.

Based on the value of R the quality of the samples can be evaluated. The lowest values of R the more disordered carbon.

Scanning electron microscopy (SEM) images of the samples were performed on Hitachi SU 8200 at 15.0 kV.

The ash content of the activated carbons was determined by standard methods (ASTM Designation D2866 11) [19]. Briefly: dried and

powdered activated carbons were burnt off for 3 h, at the temperature of 650 °C in an electric muffle furnace. The ash content was calculated by:

$$Ash\ \% = \frac{\text{Weight of solids remaining (g)}}{\text{Original weight of carbon (g)}} \bullet 100 \quad (6)$$

The X-ray fluorescence energy dispersion spectrometer (EDXRF) Epsilon3 type (Panalytical, Almelo) was used to determine the element's content in the carbon materials.

The isosteric heat of adsorption was calculated based on the Clausius-Clapeyron equation (7):

$$Q_{iso} = -R\left(\frac{\partial \ln(p)}{\partial\left(\frac{1}{T}\right)}\right)_{\theta} \quad (7)$$

where:

Q_{iso} - isosteric heat of adsorption at a constant degree of surface coverage [kJ/mol]
R - gas constant [J/mol·K]
θ - the degree of surface coverage

Upon performing differentiation on equation (7), a linear equation is obtained, indicated as equation (8):

$$\ln(p)_{\theta} = -\frac{Q_{iso}}{R}\frac{1}{T} + C \quad (8)$$

The plots of $\ln(p)_{\theta} = f(1/T)$ for the constant degree of surface coverage were made. Based on the straight-line slope values the isosteric heat of adsorption was calculated for a particular degree of surface coverage. The isosteric heat of adsorption is a very important parameter in adsorption processes. This parameter is a measure of the interaction of the adsorbate molecules with the adsorbent surface.

3. Results and discussion

3.1. Characteristics of the textural properties of activated carbons produced from common fern by CChPA

Fig. 1 shows the nitrogen adsorption isotherms at the temperature of −196 °C. All the isotherms were characterized by a rapid increase at low pressure p/p_0. This indicates that the activated carbons of the common fern are microporous materials. Hysteresis loops were narrow for activated carbons obtained at lower temperatures, sometimes even invisible without proper magnification. The presence of the hysteresis loop shows that mesopores also accompany the micropores.

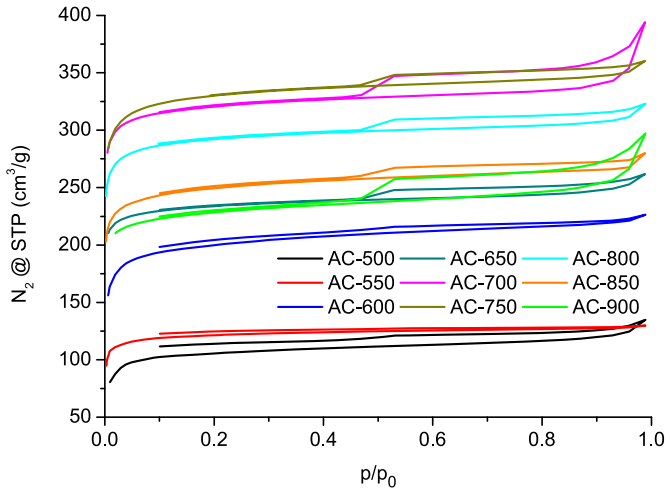

Fig. 1. Nitrogen adsorption - desorption isotherms of activated carbons produced from common fern by CChPA.

According to the IUPAC classification, all nitrogen adsorption isotherms presented in Fig. 1 combine the features of type I and type IV isotherms [20,21]. For type I, the initial shape of some isotherms can be classified as type Ia and some as Ib [22]. This course is characteristic of ordered microporous - mesoporous materials. In most of the isotherms, the restriction of adsorption at high p/p_0, characteristic of the type IV isotherm, was not observed. It can be assumed that macropores were also present in the materials in small amounts. Detailed studies on macropores have not been carried out due to the fact that these pores are irrelevant for adsorption. They are mainly used to transport the adsorbent from the outer surface to micro- and mesopores.

Hysteresis loops occurring in the tested materials are mainly of the H4 type. Some qualify as H3. Such hysteresis shapes are related to the presence of slit pores [18].

Based on nitrogen sorption measurements specific surface area (S_{BET}), total pore volume (V_{tot}) and micropore volume (V_{micN2}) were calculated, with additional estimated content of microporosity (V_{micN2}/V_{tot} and mesoporosity (V_{mes}/V_{tot}) in total pore volume. The small micropore volume (V_{micCO2}) was calculated based on CO_2 measurements. The range of micropore diameters determined by N_2 adsorption was 1.4–2 nm, and by CO_2 adsorption 0.33–1.4 nm. Table 1 showed the textural properties of activated carbons obtained from common fern.

It was found that the increase in the temperature of common fern carbonization was associated with an increase in the specific surface area, total pore volume and micropore volume determined by nitrogen adsorption. However, once a certain maximum was reached, an increase in temperature caused these values to drop. The maximum specific surface area (1016 m^2/g), the volume of pores (0.611 cm^3/g) and micropores determined by nitrogen adsorption (0.539 cm^3/g) were achieved at 700 °C. The carbon containing the most micropores determined by CO_2 adsorption (0.356 cm^3/g) was also obtained at a temperature of 700 °C.

Fig. 2a showed the pore size distribution (PSD) determined by the DFT method based on nitrogen adsorption. The method allows for determining the PSD of pores with diameters in the range of 1.4–50 nm, however, no pores with diameters larger than 3 nm were observed, therefore such a range is presented on the x-axis.

CO_2 sorption at 0 °C isotherms were used to calculate the pore size distribution (Fig. 2b) and the pore volume (0.33–1.1 nm) by the DFT method. For the activated carbons obtained from the common fern, the pore volume of narrow micropores ranged from 0.33 to 0.90 nm. In addition, the four-modal pore size distribution was observed with pore diameters of 0.35, 0.46, 0.54 and 0.82 nm.

The structure and purity of activated carbons were analysed by the XRD method. Fig. 3 showed the XRD patterns of samples prepared at temperatures in the range of 600–900 °C, two wide peaks centered at about 2θ = 23 and 43° were observed, which correspond to the plane (002) and (100/101) of the graphite structure (JCPDS 41–1487). Broad peaks indicated a highly disordered carbon structure. Similar results were obtained by Singh et al. [23]. Apart from the peaks assigned to

Table 1
Textural properties of activated carbons produced from common fern by CChPA.

Activated carbon	S_{BET} [m^2/g]	V_{tot} [cm^3/g]	V_{micN2} [cm^3/g]	V_{micCO2} [cm^3/g]
AC-500	329	0.209	0.186	0.258
AC-550	375	0.201	0.188	0.203
AC-600	622	0.351	0.321	0.186
AC-650	717	0.406	0.374	0.297
AC-700	1016	0.611	0.539	0.356
AC-750	984	0.559	0.514	0.211
AC-800	906	0.492	0.458	0.313
AC-850	771	0.434	0.396	0.257
AC-900	705	0.461	0.403	0.348

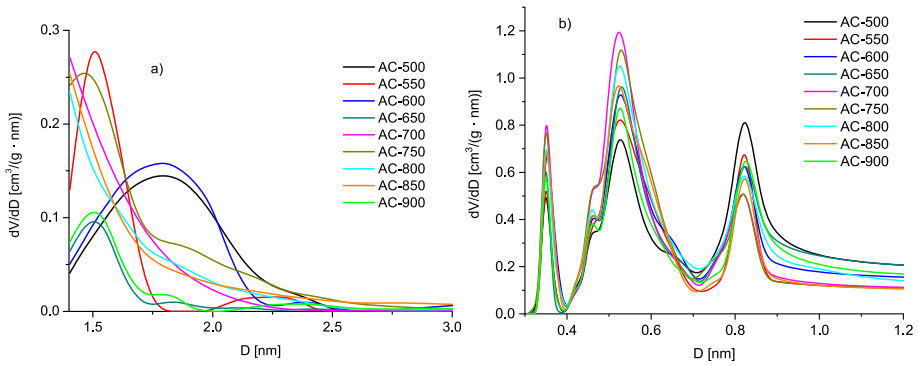

Fig. 2. Pore size distribution determined by the DFT method of activated carbons produced from common fern by CChPA (a) on the basics of N_2 sorption, (b) on the basics of CO_2 sorption.

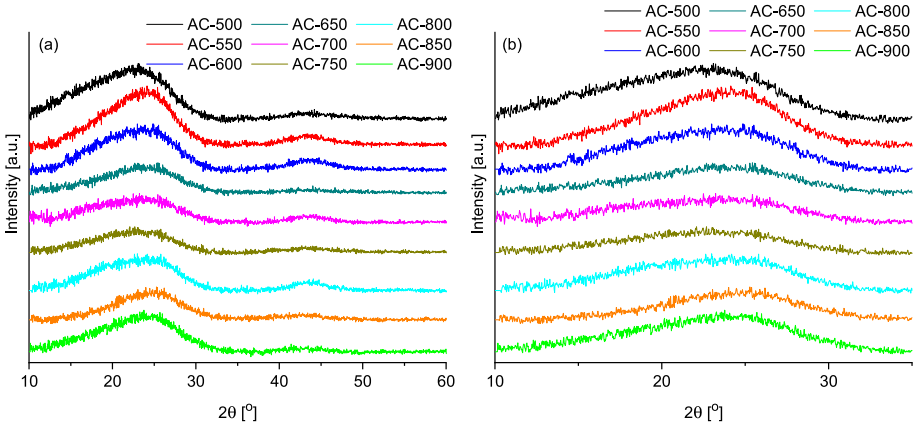

Fig. 3. XRD spectra of activated carbons produced from common fern by CChPA for a specific range of angle 2θ (a) 10–60° and (b) 10–35°.

graphite, no other peaks were visible.

For activated carbons produced in the moderate temperatures of 650–750 °C the peaks were the most flatted. That means that these materials were amorphous. Based on the peaks, height was stated that at lower and higher temperatures higher crystallinity of the samples were observed. It can be attributed to the insufficient (at lower temperatures) and extensive (at higher temperatures) reaction of KOH and CO_2 with biomass carbon. Optimizing the reaction conditions, such as the optimal temperature required for a chemical reaction, led to the formation of disordered nanoporous carbon. Therefore, their XRD peaks are wide. As a result of the application of the temperature combination, highly disordered and randomly oriented graphite carbon layers are formed (expansion of graphite carbon networks, random layer distribution, distribution of aligned structural domains), which can also be related to the large surface area, total pore volume, and micropore volume. Therefore, all these parameters play a crucial role in the efficient adsorption of CO_2. As a result of the comparison of the XRD results and the values of textural parameters (Table 1), it was found that the samples with a high degree of amorphousness showed higher porosity.

The values of the average graphite layer spacing average crystallite thickness, average graphene sheet diameter, and the average number of graphite layers are summarized in Table 2.

The average spacing between the layers (the distance between the turbostatic graphite layers) in the activated carbons was about 0.381 nm, which resulted in an increase of about 12% compared to highly ordered pyrolytic graphite. The lowest interlayer spacing (0.365 nm) was observed for activated carbon obtained at 850 °C. The highest spacing between the layers (0.393 nm) was observed for the activated carbon obtained at the temperature of 500 °C.

The higher value of the interplanar distance for activated carbons may be due to sp3 defects and/or interlayer repulsion between surfaces that are negatively charged due to surface functional groups [24]. The values of the interlayer spacing and the width of the peaks corresponding to the reflection planes (002) and (101) indicated the presence of a disordered carbon structure [25]. Note that for the AC-650, the d-distance values were not calculated as no peak was observed corresponding to (002) reflection planes. This can be associated with a much smaller value compared to other samples in the entire XRD spectra, and it is not so noticeable to observe in the graph.

The mean values of the crystallite thicknesses and the mean diameters of the graphene sheets listed in Table 2 are not exactly equal to the Lc and La of the crystallites because equation (1) was obtained for highly graphitized carbons. Therefore, it is not really suitable for turbostatic (i.e., completely disordered) carbons. Equations (3) and (4) can be used as convenient and relative estimates of the crystallite thickness

Table 2
Values of the average spacing between the graphite layers, the average thickness of the crystallites, the average diameter of the graphene sheet and the average number of graphite layers calculated from the XRD analysis.

Activated carbon	d(002) [nm]	La [nm]	Lc [nm]	N
AC-500	0.393	3.003	0.776	2.0
AC-550	0.376	3.235	0.752	2.0
AC-600	0.377	3.324	0.715	1.9
AC-650	–	–	–	–
AC-700	0.383	3.415	0.670	1.8
AC-750	0.392	–	0.713	1.8
AC-800	0.384	3.616	0.687	1.8
AC-850	0.365	–	0.706	1.9
AC-900	0.374	–	0.734	2.0

and the average diameter of the graphene sheet [26]. In fact, the crystallite sizes are probably slightly higher than those shown in Table 2. It has been found that the crystallite size values in the plane of the activated carbons are small (3.003–3.616 nm). The mean crystallite size along the c axis value was in the range of 0.670–0.776 nm, which gave the average number of graphite layers in the crystallite equal to 2.

The values shown in Table 2 confirmed the conclusions drawn based on Fig. 3 that the activated carbons synthesized at the lowest and highest temperatures showed relatively higher crystallinity. In addition, these activated carbons showed the highest average crystallite thickness, average graphene sheet diameter, and average number of graphite layers.

Activated carbons were also characterized by Raman spectroscopy to complement the XRD results (Fig. S1). The peak named G, centered around 1600 cm^{-1}, refers to graphite. In the presence of graphite disturbance in the carbon structure, a band of about 1300 cm^{-1} called D is observed. Its intensity is proportional to the number of defects. Thus, the ratio of the G and D band intensities (I_G/I_D) is used to quantify the perturbation in the crystal structure. The higher the I_G/I_D value, the less graphite perturbation. From the Raman spectra normalized to the G-band, the I_G/I_D values were estimated.

Fig. 4a showed the dependence of I_G/I_D ratio with the CChPA temperature. I_G/I_D values for common fern activated carbons ranged from 0.68 to 0.80. In the case of Lc values, they ranged from 0.67 to 0.78 (Fig. 4b). The courses of the two curves presented in Fig. 4 were similar: the highest I_G/I_D and L_c values were observed at lower and higher temperatures. The results obtained by XRD and Raman spectroscopy are pretty consistent.

The morphology of carbon materials was characterized by SEM (Fig. 5). Activated carbons prepared from fern leaves showed a sheet-assembled porous structure with typical cavities. This structure is ascribed to the pore-forming by KOH and products of the KOH with biomass reaction etching and the simultaneous oxidation by CO_2 [27]. Similar shapes were observed for the activated carbons obtained from *Camellia japonica*, *Jujun grass* [28] and *Polypodium vulgare* [42]. Further, the comprehension and establishing of the pore formation mechanism represents a crucial milestone in the fabrication of activated carbons possessing the desired characteristics, particularly the determination of the optimal activation temperature range. Based on the SEM images, elevating the carbonization temperature beyond 900 °C would lead to the degradation of the microporous architecture and the emergence of broad macropores, resulting in reduced surface area and higher weight loss [29].

To determine the purity of the obtained carbonaceous materials, the ash content in the activated carbons was determined. The ash content is the residue that remains after firing. The ash content affects the activated carbon's quality, pore volume, and surface area. High ash content leads to clogging of the pores and a reduction in the surface area and volume of the pores. Any residual mass after burning the material was attributed to the presence of mineral substances. High ash content is disadvantageous as it impedes pore development, leading to a low adsorption capacity. All activated carbons showed a low residual weight. The average ash content for activated carbons obtained from common fern was 4.50 wt%, With the highest value being 4.79 wt%. This means that the activated carbons were practically free of inorganic residues and were fully carbonaceous.

The ash content depended on the burnout of the carbon and the removal of inorganic matter due to the reaction that took place during carbonization combined with chemical and physical activation. For example, SiO_2 reacts with KOH to form water-soluble K_2SiO_3. It is removed by rinsing it with water. In this case, there is a clear downward trend in the ash content with increasing CChPA temperature (Fig. S2). In both cases, the increase in temperature likely led to a faster reaction of inorganic matter with KOH. The rate of reaction of inorganic compounds increased faster with temperature than the rate of coal combustion. The ash content values were consistent with the XRF results (Table S1). Similar results for activated carbons obtained from biomass were also obtained by Smirti et al. [30].

During carbonization combined with chemical and physical activation, a lot of chemical reactions took place. Through the reaction of KOH with biomass K_2CO_3, H_2O, H_2, K, and CO were produced. The onset temperature for the redox reaction between potassium hydroxide (KOH) and carbon precursors is estimated to be around 400 °C, resulting in the formation of potassium carbonate (K_2CO_3). At approximately 600 °C, KOH undergoes complete conversion into K_2CO_3. At temperatures exceeding 700 °C, the compound K_2CO_3 undergoes thermal decomposition, resulting in the formation of carbon dioxide (CO_2) and potassium oxide (K_2O). The main reactions with KOH and biomass were as follows:

$$2\ KOH + C + H_2O \rightarrow K_2CO_3 + 2H_2$$

$$6\ KOH + 2\ C \rightarrow 2\ K_2CO_3 + 2\ K + 3H_2$$

$$4\ KOH + C \rightarrow K_2CO_3 + H_2O + 2H_2$$

$$2\ KOH + 2C \rightarrow 2CO + 2\ K + H_2$$

The decomposition of chemical activating agent took also place:

$$2KOH \rightarrow K_2O + H_2O$$

The physical activating agent reacted with biomass too:

$$C + CO_2 \rightarrow 2CO$$

and with chemical activating agent:

$$2\ KOH + CO_2 \rightarrow K_2CO_3 + H_2O$$

The resulting gasses are influenced by the porosity and the structure of the activated carbons. The products of the reactions presented above: K_2CO_3, K_2O also reacted with the biomass and influenced the final

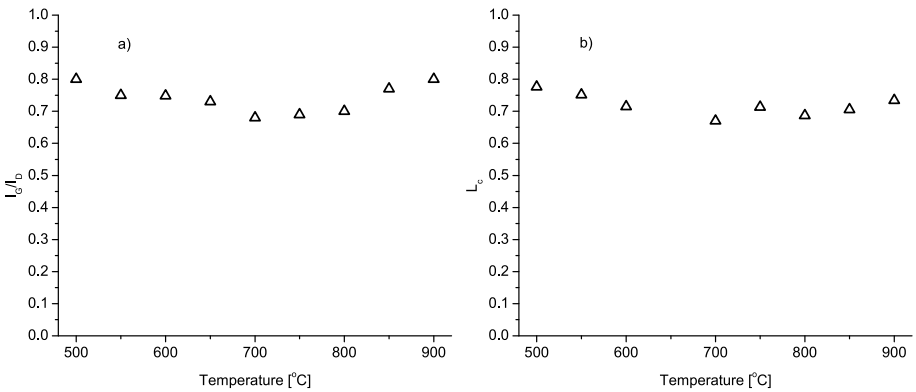

Fig. 4. Effect of synthesis temperature on (a) I_G/I_D and (b) Lc value for activated carbons produced from common fern by CChPA.

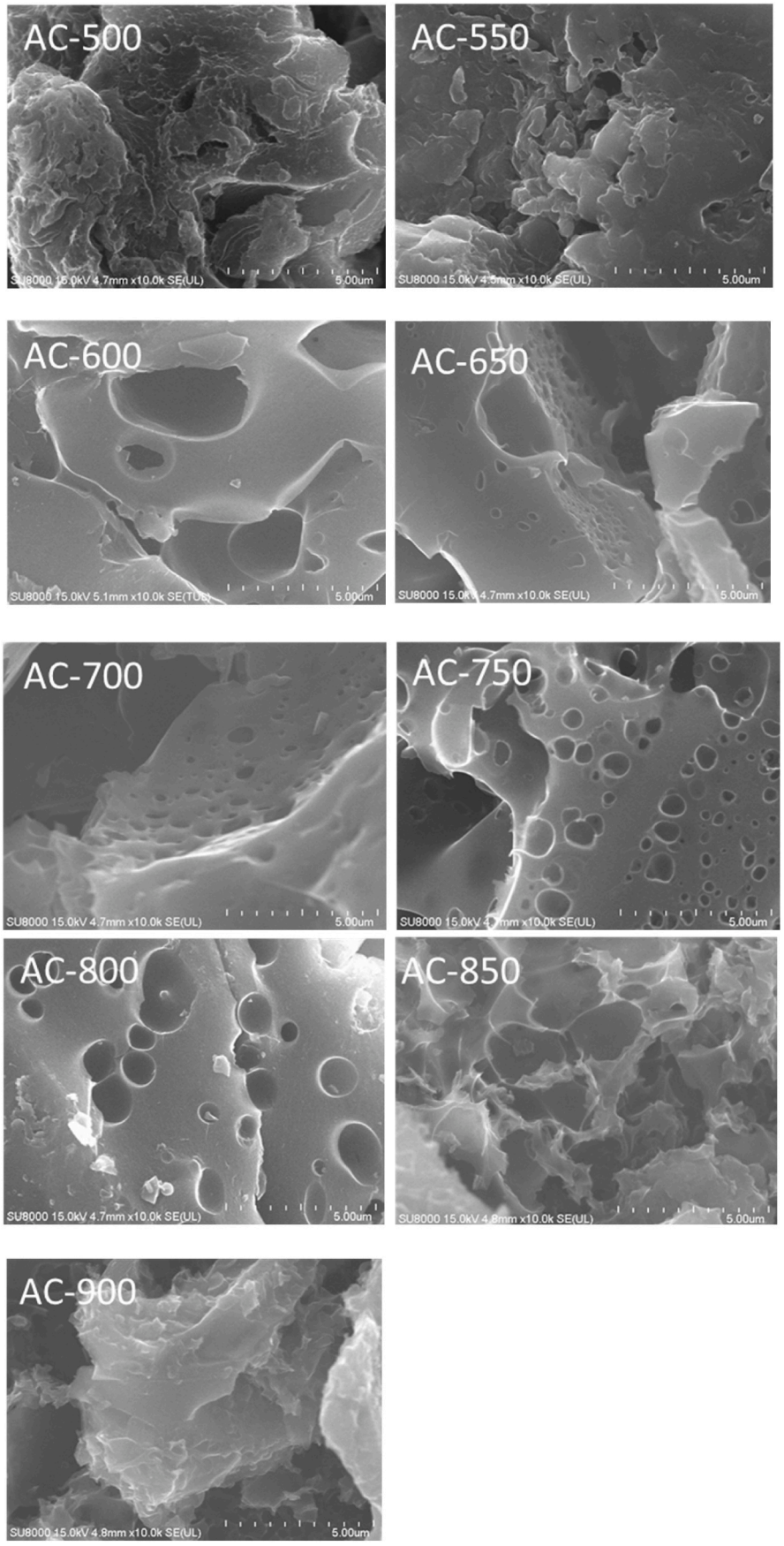

Fig. 5. SEM images of activated carbons produced from common fern by CChPA.

product.

Due to the complicated reactions that take place simultaneously during the process, only the temperature changes led to activated carbons showing different properties.

3.2. Adsorption of CO_2 and selectivity CO_2 on N_2

Fig. 6 showed the CO_2 adsorption isotherms at 0 °C (a) and 25 °C (b) at pressures up to 100 kPa. The CO_2 adsorption isotherms at 0 °C and 25 °C increased sharply at low pressure and slowly became less steep at higher pressures. The highest CO_2 adsorption under the pressure of 100 kPa was achieved for the activated carbon obtained at the temperature of 700 °C. The adsorption of carbon dioxide at 100 kPa pressure on AC-700 was 6.76 and 3.58 mmol/g, at temperatures of 0 °C and 25 °C, respectively (Table S2). Table S2 presented CO_2 adsorption on all the activated carbons obtained from fern at a pressure of 100 kPa and a temperature of 0 °C and 25 °C. Table 3 showed high CO_2 adsorption on activated carbons produced from biomass described by other authors. Considering the values from Table 3 and Table S2 was stated that all the activated carbons produced from common fern by CChPA were very good CO_2 sorbents.

At the temperature of 0 °C, the adsorption of CO_2 was higher than at 25 °C for all activated carbons. The decreasing adsorption with increasing temperature is widely described in the literature. This indicates the physisorption and exothermic nature of CO_2 sorption on activated carbons obtained from fern. The van der Waals forces played a fundamental role in the interaction between CO_2 and activated carbons. These molecular forces are quite strong at low temperatures, but they weaken as the temperature increases. This is also in line with Le Chatelier's principle.

It was assumed that the CO_2 adsorption capacity at 100 kPa may depend on the surface area the total pore volume, the micropore volume determined by nitrogen (V_{micN2}) and small micropores determined by CO_2 (V_{micCO2}). Fig. S3 presented the CO_2 adsorption as a linear function of S_{BET}, V_{tot}, V_{micN2} and V_{micCO2}. The analysis of the coefficient of determination values indicated the strongest linear relationship between CO_2 adsorption and specific surface area volume values for both 0 and 25 °C temperatures. Similar results were presented by Ouzzine et al. [42]. However, it should be noted that the coefficient of determination values was also very high for the micropore volume in the range of 1.4–2 nm. Probably both surface area and micropore volume played a significant role in the adsorption of CO_2 at temperatures of 0 and 25 °C at the pressure of 100 kPa.

The isosteric heat of adsorption (Q_{iso}) value is important for characterizing the interaction between the adsorbent and the adsorbate. It gives information on the strength of the adsorption. A higher Q_{iso} value indicates a stronger interaction between carbon dioxide and activated carbons. The high isosteric heat of adsorption causes a high cost of regeneration. The isosteric heat of CO_2 adsorption of activated carbons as a function of the degree of surface coverage was shown in Fig. 7. The isosteric heat of adsorption values for common fern activated carbons ranged from 27 to 32 kJ/mol for surface coverage in the range 0.1–0.35. These values strongly confirmed the physical nature of CO_2 sorption on activated carbons. The typical energies for physisorption are in the range

Table 3
CO_2 adsorption on activated carbons produced from biomass at 100 kPa, 0 °C and 25 °C.

Activated Carbon	CO_2 adsorption at 0 °C [mmol/g]	CO_2 adsorption at 25 °C [mmol/g]	References
rice husk	5.83	–	[31]
tea sead shell	–	3.15	[32]
pine cone	6.57	–	[33]
walnut shell	5.22	3.06	[34]
coconut shell	6.04	4.23	[35]
birch	4.50	4.06	[36]
palm sheath	5.28	3.48	[37]
cellulose	6.75	3.96	[38]
pomegranate peels	3.90	2.36	[39]
corn cobs	2.70	2.31	[35]
peanut shells	5.20	4.51	[35]
common oak leaves	6.17	5.44	[40]
andiroba shells	6.10	3.20	[41]
fern leaves (AC-700)	6.77	3.58	This work

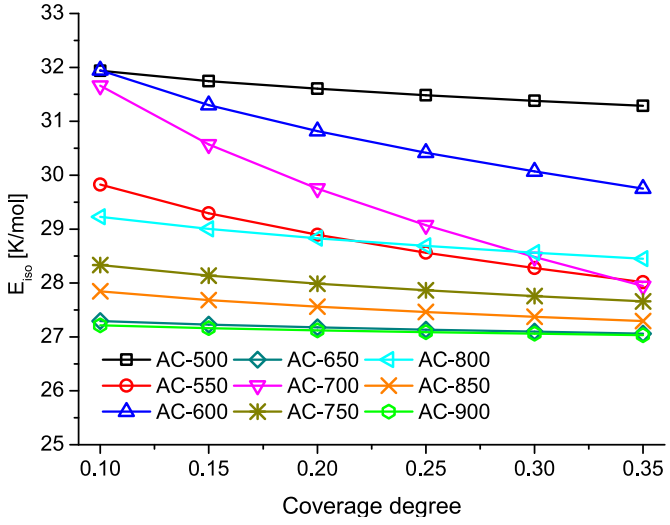

Fig. 7. The isosteric heat of CO_2 adsorption calculated based on CO_2 adsorption at 0 °C and 25 °C.

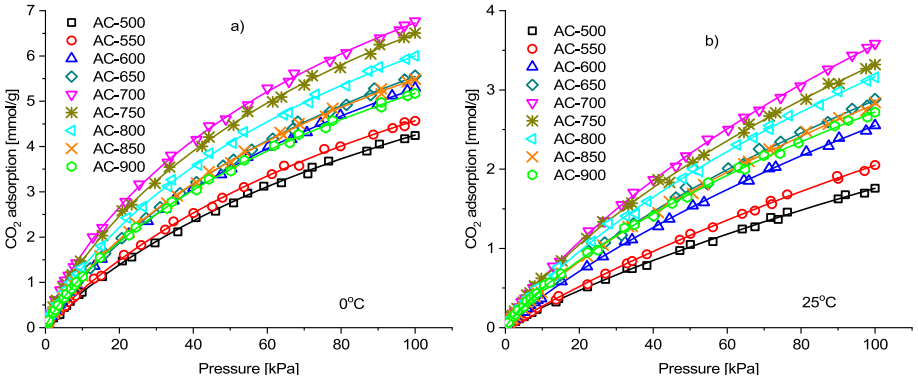

Fig. 6. Carbon dioxide adsorption isotherms at temperatures of (a) 0 °C and (b) 25 °C on activated carbons produced from common fern by CChPA.

of 20–40 kJ/mol, while the range of 80–400 kJ/mol is characteristic for chemisorption [43]. The isosteric heat of adsorption decreased with the coverage of the surface. The greater the surface coverage, the weaker the interaction between carbon dioxide and activated carbons. It is evident that carbon dioxide was bound to the surface of the activated carbons by van der Waals forces and can be easily desorbed. The values of the isosteric heat of CO_2 adsorption of activated carbons were low. Such values are highly desirable for post-combustion capture because of their regeneration costs [44].

Selectivity is important when assessing sorbents for CO_2 removal from flue gases. Nitrogen adsorption isotherms were measured at 25 °C, up to a pressure of 100 kPa (Fig. S4) N_2 adsorption values obtained by activated carbons were below 0.25 mmol/g.

The selectivity of CO_2 over N_2 was calculated based on the ideal adsorbed solution theory (IAST) [45]. According to the IAST, for the binary mixtures of A and B compounds, the adsorption selectivity of A over B can be calculated based on single adsorption isotherms of A and B, according to equation (9):

$$S_{IAST(A)} = \frac{\frac{x_A}{y_A}}{\frac{x_B}{y_B}} \tag{9}$$

where:

x_A and x_B – the molar fractions of A and B compound in the adsorbed phase

y_A and y_B – the molar fractions of A and B compound in the bulk phase.

Based on the IAST method the selectivity of A over B for any content of the compounds in a binary mixture can be calculated. The accuracy of the IAST method was confirmed for numerous gas mixtures on a lot of sorbents [46,47].

In order to calculate the selectivity of CO_2 over N_2 based on the IAST equation (9) has been converted to equation (10):

$$S_{IAST(CO_2)} = \frac{q_{CO_2(p_{CO2})}}{p_{CO_2}} : \frac{q_{N_2(p_{N2})}}{p_{N_2}} \tag{10}$$

where: $q_i(p)$ - adsorption capacity of i at pressure pi.

According to the IAST for equimolar CO_2 and N_2 mixture the adsorption selectivity (S_{CO2}) was calculated by dividing the CO_2 adsorption capacity by the N_2 adsorption capacity at 25 °C using equation:

$$S_{CO_2} = \frac{q_{CO_2(p)}}{q_{N_2(p)}} \tag{11}$$

where: $q_i(p)$ is the carbon dioxide and nitrogen adsorption at the same partial pressure p. The adsorption selectivity (S_{CO2}) for the equimolar CO_2 and N_2 mixture was presented in Fig. 8.

The CO_2/N_2 selectivity at low pressure was equal to 500–600 and then dropped very quickly down to a pressure of about 20 kPa. For pressures greater than 20 kPa, a slow increase in selectivity for CO_2/N_2 was observed. The selectivity values at the pressure of 100 kPa were ranged from 21 to 30 (Table S2). They were quite high compared to others described in the literature [48,49].

The IAST was also used to calculate the selectivity of CO_2 over N_2 for a typical flue gas mixture, namely 15% CO_2 and 85% N_2. The CO_2 selectivity for a typical flue gas mixture was calculated according to the equation:

$$S_{CO_2(FG)} = \frac{q_{CO_2(15kPa)}}{q_{N_2(85kPa)}} \times \frac{85}{15} \tag{12}$$

The selectivity of CO_2 over N_2 for a typical flue gas mixture was presented in Table S2. The $S_{CO2(FG)}$ values for the fern activated carbons ranged from 45.7 to 57.2. The obtained values were similar to those

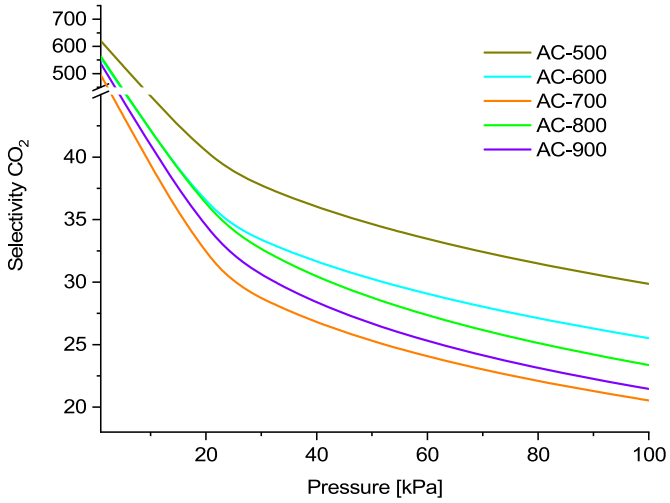

Fig. 8. CO_2 selectivity for equimolar mixture of CO_2/N_2 at 25 °C as a function of the pressure.

received for activated carbons from various biomass sources [50,51]. In the case of purely physically adsorptive selectivity, the separation is dependent on various physical properties of the gas molecules, such as polarizability or a quadrupole moment, which leads to a higher enthalpy of adsorption of some molecules compared to others ones. Since the polarizability (CO_2, 29.1 10^{-25} cm^{-3}; N_2, 17.4 10^{-25} cm^{-3}) ad quadrupole moment (CO_2, 13.4 10^{-40} C m^2; N_2, 4.7 10– 40 C m^2) of CO_2 are higher than those of N_2, it is expected that a high selectivity [52–54].

4. Conclusion

The one step sustainable technology of activated carbon production was applied in this work. This promising approach aims to address the environmental impact associated with traditional methods while ensuring the efficient and cost-effective production of high-quality activated carbon. The carbonization and chemical and physical activation were performed in the oven at the same time giving savings of energy and resources.

By changing the temperature of activated carbons production in the range of 500–900 °C the properties of obtained materials, especially porosity and carbonaceous structure, can be tailored. The best properties for the high CO_2 adsorption were high specific surface area, micropore volume in the range 1.4–2 nm and amorphous structure.

The activated carbon prepared at the temperature of 700 °C showed the highest CO_2 adsorption at the pressure of 100 kPa: 6.77 mmol/g and 3.58 mmol/g at the temperature of 0 and 25 °C respectively. This sorbent was amorphous and had the highest micropore volume. The second highest CO_2 adsorption was observed on activated carbon obtained at the temperature of 750 °C (6.51 mmol, 3.32 mmol/g). This material was also amorphous and had the highest specific surface area volume.

The selectivities of CO_2 over N_2 calculated using IAST method were also high, making carbon produced from fern promising sorbents, especially for CO_2 removing from flue gas.

Data availability

The data that has been used is confidential.

Acknowledgements

Jarosław Serafin is grateful to Spanish Ministry of Research and Innovation project no: PID2020-116031RBI00/AEI/10.13039/501100011033/FEDER.

Appendix A. Supplementary data

Supplementary data to this article can be found online at https://doi.org/10.1016/j.biombioe.2023.106880.

References

[1] K. Roa, E. Oyarce, A. Boulett, M. Alsamman, D. Oyarzún, G.D.C. Pizarro, J. Sánchez, Lignocellulose-based materials and their application in the removal of dyes from water: a review, Sustain. Mater. Technol. 29 (2021), e00320, https://doi.org/10.1016/j.susmat.2021.e00320.

[2] L.K.C. de Souza, A.A.S. Gonçalves, L.S. Queiroz, J.S. Chaar, G.N. da Rocha Filho, C. E.F. da Costa, Utilization of acai stone biomass for the sustainable production of nanoporous carbon for CO2 capture, Sustain. Mater. Technol. 25 (2020), e00168, https://doi.org/10.1016/j.susmat.2020.e00168.

[3] J. Młodzik, J. Sreńscek-Nazzal, U. Narkiewicz, A.W. Morawski, R.J. Wróbel, B. Michalkiewicz, Activated carbons from molasses as CO 2 sorbents, Acta Phys. Pol. 129 (2016) 402–404, https://doi.org/10.12693/APhysPolA.129.402.

[4] G. Singh, K.S. Lakhi, S. Sil, S.V. Bhosale, I. Kim, K. Albahily, A. Vinu, Biomass derived porous carbon for CO2 capture, Carbon N. Y. 148 (2019) 164–186, https://doi.org/10.1016/j.carbon.2019.03.050.

[5] B. Dziejarski, R. Krzyżyńska, K. Andersson, Current status of carbon capture, utilization, and storage technologies in the global economy: a survey of technical assessment, Fuel 342 (2023), 127776, https://doi.org/10.1016/j.fuel.2023.127776.

[6] B. Jiang, Q. Sun, B. Guene Lougou, H. Zhang, X. Li, Z. Qu, Y. Shuai, C.-H. Wang, Highly-selective CO2 conversion through single oxide CuO enhanced NiFe2O4 thermal catalytic activity, Sustain. Mater. Technol. 32 (2022), e00441, https://doi.org/10.1016/j.susmat.2022.e00441.

[7] Z.H. Lee, K.T. Lee, S. Bhatia, A.R. Mohamed, Postcombustion carbon dioxide capture: evolution towards utilization of nanomaterials, Renew. Sustain. Energy Rev. 16 (2012) 2599–2609, https://doi.org/10.1016/j.rser.2012.01.077.

[8] J. Liu, P.K. Thallapally, B.P. Mcgrail, D.R. Brown, J. Liu, Progress in adsorption-based CO2 capture by metal-organic frameworks, Chem. Soc. Rev. 41 (2012) 2308–2322, https://doi.org/10.1039/C1CS15221A.

[9] A. Bakhtyari, M. Mofarahi, Ch H. Lee, Chapter 9 - CO2 adsorption by conventional and nanosized zeolites, Advances in Carbon Capture (2022) 193–228, https://doi.org/10.1016/B978-0-12-819657-1.00009-8.

[10] J. Qian, F. Jiang, D. Yuan, M. Wu, S. Zhang, L. Zhang, M. Hong, Highly selective carbon dioxide adsorption in a water-stable indium-organic framework material, Chem. Commun. 48 (2012) 9696–9698, https://doi.org/10.1039/C2CC35068H.

[11] A.L. Khan, C. Klaysom, A. Gahlaut, X. Li, I.F.J. Vankelecom, SPEEK and functionalized mesoporous MCM-41 mixed matrix membranes for CO2 separation, J. Mater. Chem. 22 (2012) 20057–20064, https://doi.org/10.1039/C2JM34885C.

[12] W. Kukulka, K. Cendrowski, B. Michalkiewicz, E. Mijowska, MOF-5 derived carbon as material for CO2 absorption, RSC Adv. 9 (2019) 18527–18537, https://doi.org/10.1039/C9RA01786K.

[13] L. Li, T. Wang, Q. Liu, Y. Cao, J. Qiu, A high CO2 permselective mesoporous silica/carbon composite membrane for CO2 separation, Carbon 50 (2012) 5186–5195, https://doi.org/10.1016/j.carbon.2012.06.060.

[14] I.S. Ismail, N.A. Rashidi, S. Yusup, Production and characterization of bamboo-based activated carbon through single-step H3PO4 activation for CO2 capture, Environ. Sci. Pollut. Res. 29 (2022) 12434–12440, https://doi.org/10.1007/s11356-021-15030-x.

[15] F. Mbarki, T. Selmi, A. Kesraoui, M. Seffen, Low-cost activated carbon preparation from Corn stigmata fibers chemically activated using H3PO4, ZnCl2 and KOH: study of methylene blue adsorption, stochastic isotherm and fractal kinetic, Ind. Crop. Prod. 178 (2022), 114546, https://doi.org/10.1016/j.indcrop.2022.114546.

[16] A. Vasco, R.C. Moran, B.A. Ambrose, The evolution, morphology, and development of fern leaves, Front. Plant Sci. 4 (2013) 345, https://doi.org/10.3389/fpls.2013.00345.

[17] B.D. Cullity, S.R. Stock, Elements of X-Ray Diffraction, MA, 1978, p. 828.

[18] L. Lu, V. Sahajwalla, C. Kong, D. Harris, Quantitative X-ray diffraction analysis and its application to various coals, Carbon 39 (2001) 1821–1833, https://doi.org/10.1016/S0008-6223(00)00318-3.

[19] ASTM D2866-11, Standard Test Method for Total Ash Content of Activated Carbon, ASTM International, West Conshohocken, PA, 2018, 2018.

[20] K.S.W. Sing, D.H. Everett, R.A.W. Haul, L. Moscou, R.A. Pierotti, J. Rouquerol, T. Siemienewska, Reporting physisorption data for gas solid systems with special reference to the determination of surface-area and porosity, Pure Appl. Chem. 57 (1985) 603–619, https://doi.org/10.1351/pac198557040603.

[21] J. Serafin, B. Dziejarski, Application of isotherms models and error functions in activated carbon CO2 sorption processes, Microporous Mesoporous Mater. 354 (2023), 112513, https://doi.org/10.1016/j.micromeso.2023.112513.

[22] M. Thommes, K. Kaneko, A.V. Neimark, J.P. Olivier, F. Rodriguez-Reinoso, J. Rouquerol, K.S.W. Sing, Physisorption of gases, with special reference to the evaluation of surface area and pore size distribution (IUPAC Technical Report), Pure Appl. Chem. 87 (2015) 1051–1069, https://doi.org/10.1515/pac-2014-1117.

[23] G. Singh, K.S. Lakhi, K. Ramadass, S. Kim, D. Stockdale, A. Vinu, A combined strategy of acid-assisted polymerization and solid state activation to synthesize functionalized nanoporous activated biocarbons from biomass for CO_2 capture, MicroporMesopor Mat 271 (2018) 23–32, https://doi.org/10.1016/j.micromeso.2018.05.035.

[24] A. Ghosh, C. Amaral Razzino, A. Dasgupta, K. Fujisawa, L.H.S. Vieira, S. Subramanian, R.S. Costa, A.O. Lobo, O.P. Ferreira, J. Robinson, M. Terrones, H. Terrones, B.C. Viana, Structural and electrochemical properties of babassu coconut mesocarp-generated activated carbon and few-layer Graphene, Carbon 149 (2019) 175–186, https://doi.org/10.1016/j.carbon.2018.12.114.

[25] Z.L. Yaneva, B.K. Koumanova, N.V. Georgieva, Linear Regression and Nonlinear Regression Methods for Equilibrium Modelling of P – Nitrophenol Biosorption by Rhyzopus Oryzen: Comparison of Error Analysic Criteria, J. Chem – NY., 2013, https://doi.org/10.1155/2013/517631. Article ID 517631.

[26] B.S. Girgis, Y.M. Temerk, M.M. Gadelrab, I.D. Abdullah, X – ray diffraction patterns of activated carbons prepared under various conditions, Carbon Science 8 (2007) 95–100, https://doi.org/10.5714/CL.2007.8.2.095.

[27] M. Sevilla, R. Mokaya, Energy storage applications of activated carbons: supercapacitors and hydrogen storage, Energy Environ. Sci. 7 (2014) 1250–1280, https://doi.org/10.1039/C3EE43525C.

[28] H. Matabosch Coromina, D.A. Walsh, R. Mokaya, Biomass – derived activated carbon with simultaneously enhanced CO2 uptake for both pre and post combustion capture applications, J. Mater. Chem. 4 (2016) 280–289, https://doi.org/10.1039/C5TA09202G.

[29] J. Serafin, B. Dziejarski, O.F.C. Junior, J. Sreńscek-Nazzal, Design of highly microporous activated carbons based on walnut shell biomass for H2 and CO2 storage, Carbon 201 (2023) 633–647, https://doi.org/10.1016/j.carbon.2022.09.013.

[30] S. Chettri, S. Manivannan, V.R. Muddarsu, Nutrient and elemental composition of wild edible ferns of the himalaya, Am. Fern J. 108 (2018) 95–106, https://doi.org/10.1640/0002-8444-108.3.95.

[31] S. He, G. Chen, H. Xiao, G. Shi, C. Ruan, Y. Ma, H. Dai, B. Yuan, X. Chen, X. Yang, Facile preparation of N-doped activated carbon produced from rice husk for CO2 capture, J. Colloid Interface Sci. 582 (2021) 90–101, https://doi.org/10.1016/j.jcis.2020.08.021.

[32] C. Quan, X. Jia, N. Gao, Nitrogen-doping activated biomass carbon from tea seed shell for CO2 capture and supercapacitor, Int. J. Energy Res. 44 (2020) 1218–1232, https://doi.org/10.1002/er.5017.

[33] C.H. Kim, S.Y. Lee, S.J. Park, Efficient micropore sizes for carbon dioxide physisorption of pine cone-based carbonaceous materials at different temperatures, J. CO2 Util. 54 (2021), 101770, https://doi.org/10.1016/j.jcou.2021.101770.

[34] Z. Yang, G. Zhang, Y. Xu, P. Zhao, One step N-doping and activation of biomass carbon at low temperature through NaNH2: an effective approach to CO2 adsorbents, J. CO2 Util. 33 (2019) 320–329, https://doi.org/10.1016/j.jcou.2019.06.021.

[35] J. Yang, L. Yue, X. Hu, L. Wang, Y. Zhao, Y. Lin, Y. Sun, H. DaCosta, L. Guo, Efficient CO2 capture by porous carbons derived from coconut shell, Energy Fuels 31 (2017) 4287–4293, https://doi.org/10.1021/acs.energyfuels.7b00633.

[36] K.K. Kishibayev, J. Serafin, R.R. Tokpayev, T.N. Khavaza, A.A. Atchabarova, D. A. Abduakhytova, Z.T. Ibraimov, J. Sreńscek-Nazzal, Physical and chemical properties of activated carbon synthesized from plant wastes and shungite for CO_2 capture, J. Environ. Chem. Eng. 9 (2021), 106798, https://doi.org/10.1016/j.jece.2021.106798.

[37] Y. Zhang, Z. Wei, X. Liu, Z. Yan, S. Zhou, J. Wang, S. Deng, Synthesis of palm sheath derived- porous carbon for selective CO2 adsorption, RSC Adv. 12 (2022) 8592–8599, https://doi.org/10.1039/D2RA00139J.

[38] U. Kamran, S.-J. Park, Acetic acid-mediated cellulose-based carbons: influence of activation conditions on textural features and carbon dioxide uptakes, J. Colloid Interface Sci. 594 (2021) 745–758, https://doi.org/10.1016/j.jcis.2021.03.069.

[39] H. Mumtaz, M. Farhan, M. Amjad, Biomass waste utilization for adsorbent preparation in CO2 capture and sustainable environment applications, Sustain. Energy Technol. Assessments 46 (2021), 101288, https://doi.org/10.1016/j.seta.2021.101288.

[40] J. Serafin, O.F. Cruz Jr., Promising activated carbons derived from common oak leaves and their application in CO2 storage, J. Environ. Chem. Eng. 10 (2022), 107642, https://doi.org/10.1016/j.jece.2022.107642.

[41] J. Serafin, M. Ouzzine, C. Xing, H. El Ouahabi, A. Kamińska, J. Sreńscek-Nazzal, Activated carbons from the Amazonian biomass andiroba shells applied as a CO2 adsorbent and a cheap semiconductor material, J. CO2 Util. 62 (2022), 102071, https://doi.org/10.1016/j.jcou.2022.102071.

[42] M. Ouzzine, J. Serafin, J. Sreńscek-Nazzal, Single step preparation of activated biocarbons derived from pomegranate peels and their CO2 adsorption performance", J. Anal. Appl. Pyrolysis 160 (2021), 105338 https://doi.org/10.1016/j.jaap.2021.105338.

[43] X. Zhou, H. Yi, X. Tang, H. Deng, H. Liu, Thermodynamics for the adsorption of SO2, NO and CO2 from flue gas on activated carbon fiber, Chem. Eng. J. 200 (2012) 399–404, https://doi.org/10.1016/j.cej.2012.06.013.

[44] J.M. Simmons, H. Wu, W. Zhou, T. Yildirim, Carbon capture in metal–organic frameworks—a comparative study, Energy Environ. Sci. 4 (2011) 2177–2185, https://doi.org/10.1039/C0EE00700E.

[45] A.L. Myers, J.M. Prausnitz, Thermodynamics of mixed-gas adsorption, AIChE J. 11 (1965) 121–127, https://doi.org/10.1002/aic.690110125.

[46] Z.R. Herm, J.A. Swisher, B. Smit, R. Krishna, J.R. Long, Metal−Organic frameworks as adsorbents for hydrogen purification and precombustion carbon dioxide capture, J. Am. Chem. Soc. 133 (2011) 5664–5667, https://doi.org/10.1021/ja111411q.

[47] W. Lu, D. Yuan, J. Sculley, D. Zhao, R. Krishna, H.-C. Zhou, Sulfonate-grafted porous polymer networks for preferential CO2 adsorption at low pressure, J. Am. Chem. Soc. 133 (2011) 18126–18129, https://doi.org/10.1021/ja2087773.

[48] Y. Zhu, J. Gao, Y. Li, F. Sun, J. Gao, S. Wu, Y. Qin, Preparation of activated carbons for SO2 adsorption by CO2 and steam activation, J. Taiwan Inst. Chem. Eng. 43 (2012) 112–119, https://doi.org/10.1016/j.jtice.2011.06.009.

[49] J. Serafin, S. Vikram, B. Dziejarski, S. Sahoo, An environmentally friendly synthesis method of activated carbons based on subabul (Leucaena leucocephala) sawdust waste for CO2 adsorption, J. Clean. Prod. 412 (2023), 137406, https://doi.org/10.1016/j.jclepro.2023.137406.

[50] Z.L. Yaneva, B.K. Koumanova, N.V. Georgieva, Linear Regression and Nonlinear Regression Methods for Equilibrium Modelling of P – Nitrophenol Biosorption by Rhyzopus Oryzen: Comparison of Error Analysic Criteria, J. Chem – NY., 2013, https://doi.org/10.1155/2013/517631. Article ID 517631.

[51] J. Serafin, K. Kiełbasa, B. Michalkiewicz, The new tailored nanoporous carbons from the common polypody (Polypodium vulgare): the role of textural properties for enhanced CO2 adsorption, Chem. Eng. J. 429 (2022), 131751, https://doi.org/10.1016/j.cej.2021.131751.

[52] H.M. Coromina, D.A. Walsh, R. Mokaya, Biomass-derived activated carbon with simultaneously enhanced CO2 uptake for both pre and post combustion capture applications, J. Mater. Chem. A. 4 (2016) 280–289, https://doi.org/10.1039/C5TA09202G.

[53] J. Serafin, M. Ouzzine, O.F. Cruz Junior, J. Srenscek-Nazzal, Preparation of lowcost activated carbons from amazonian nutshells for CO2 storage, Biomass Bioenergy 144 (2021), https://doi.org/10.1016/j.biombioe.2020.105925.

[54] S. Keskin, T.M. van Heest, D.S. Sholl, Can metal-organic framework materials play a useful role in large-scale carbon dioxide separations? ChemSusChem 3 (2010) 879–891, https://doi.org/10.1002/cssc.201000114.